Neutral Recycling Effect on Edge ITG Turbulence and Transport

D. P. Stotler[1], J. Lang[2], C. S. Chang[1] and S. Ku[1]

[1]Princeton Plasma Physics Laboratory, Princeton University, Princeton, NJ 08543-451, USA
[2]Intel Corporation, Santa Clara, USA

Corresponding Author: dstotler@pppl.gov

Abstract:
The effects of recycled neutral atoms on tokamak ion temperature gradient (ITG) turbulence have been investigated in a steep edge pedestal, magnetic separatrix configuration with the full-f edge gryokinetic code XGC1. ITG turbulence is the most fundamental and robust instability, having a long radial correlation length and an ability to impact other forms of pedestal turbulence. The charge exchange interactions of the atoms with the plasma ions enhance the ITG turbulence, first, by increasing the ion temperature gradient in the pedestal region and, second, by reducing the $E \times B$ shearing rate.

1 Introduction

ITER and other future burning plasma devices are expected to operate in the high confinement mode, or H-mode. Yet, the means by which a tokamak initially in the low confinement regime (L-mode) transitions into H-mode (L-H) is not well understood, nor are the mechanisms that suppress the turbulence and maintain the steep gradients in the H-mode. Although the effects of neutral particles (e.g., due to recycling) on core plasma fueling are more frequently discussed, their impact on plasma turbulence, the L-H transition, and H-mode remain open areas of investigation, theoretically [1, 2] and experimentally [3, 4]. For example, the role of neutral atoms in the processes that set the L-H threshold power has been the focus of multiple theoretical models [5, 6, 7, 8, 9]. That neutrals affect the L-H transition has also been demonstrated experimentally [10, 11, 12, 13, 14]. The momentum and energy losses associated with neutral-ion interaction have been quantified [15, 16]. However, direct numerical simulation of the effects of neutrals on plasma instabilities and turbulence has previously been impractical due to the associated computational and algorithmic challenges.

The most relevant plasma-atom interactions are electron impact ionization and resonant charge exchange (CX). Hydrogen molecules released from plasma facing surfaces by various plasma interaction processes, referred to collectively as "recycling", are dissociated and / or ionized close to the walls; only the relatively energetic product atoms (~ 3

eV) have mean free paths long enough to penetrate inside closed flux surfaces. Because such atoms are inevitably migrating into a region with hotter ions, subsequent CX interactions have a cooling effect on the ion distribution. Moreover, the finite widths of the ion banana orbits cause this cooling to be felt beyond the location of the CX collision. The increased energies of the resulting atoms lead to even longer mean free paths and, thus, deeper penetration into the confined plasma [17]. Note that the eventual ionization of these atoms represents a local power source for the ions, offsetting some of the charge exchange cooling [16]. The multistep excitation, de-excitation, radiative decay, and ionization processes contributing to the collisional radiative "ionization" of a particular atom [18] also represent a significant power sink for the electron population, although it is not considered in this investigation. Electron-ion recombination can be a significant or even dominant process in high density, low temperature (< 1 eV) divertor plasmas, but is of little relevance to instabilities in the edge plasma.

One obvious consequence of the pedestal CX cooling is a steepening of the ion temperature profile and an associated enhancement in gradient driven instabilities and turbulence. However, neutrals can also impact the $E \times B$ shear flows that are critical in determining the potency of turbulent fluctuations [2, 6]. In this paper, we use the full-f, particle-in-cell code XGC1 [19, 20, 21, 22] to investigate how both phenomena impact ion temperature gradient (ITG) driven turbulence. Essential to this investigation is XGC1's ability to simulate the entire plasma from the magnetic axis to the material walls in a realistic separatrix geometry, typically specified via a numerical equilibrium in the EFIT EQDSK format [23]. The boundary conditions at the material surfaces intersected by open field lines are set via a logical sheath criterion [24] in a typical XGC1 simulation. However, with the adiabatic electron model used in these simulations, the plasma potential is set to zero in the entire scrape-off layer (SOL). This simplifying assumption is not expected to affect our results given that penetration of the ITG turbulence into the SOL is weak. Neutral particles resulting from the subsequent plasma-material interaction are consistently simulated with a built-in Monte Carlo procedure, described below. Charged particle collisions are effected by a nonlinear Fokker-Planck-Landau collision operator [25, 26]. XGC1 also allows the specification of additional heat, momentum, and particle sources (e.g., neutral beam injection).

The neutral transport model used by XGC1 is described in Sec. 2. The simulations, one without recycling, as if the walls were purely absorbing, and one with an experimentally relevant 99% recycling, are described in Sec. 3. The effects of the assumed recycling model on the plasma profiles and turbulence are examined in that same section. Our conclusions are presented in Sec. 4.

2 Neutral Transport Model

Two neutral transport models are available within the XGC code family. The most sophisticated is accessed via a subroutine interface to the DEGAS 2 Monte Carlo neutral transport code [27, 28]. The other traces back to the built-in routine in the original XGC [19], to which improvements have been made [29]. The former allows the incorporation of detailed models for plasma-material interactions and additional neutral species, e.g., molecules. Given the focus of the present work on the confined plasma, that added complexity is superfluous, and the built-in model, which treats only atoms, will suffice.

Both models utilize a "test particle" Monte Carlo approach for dealing with the non-linearity of the neutral-plasma collision operator [28] that involves two complementary plasma-neutral collision routines. In the first, kinetic neutrals collide off a fluid plasma background obtained from the kinetic particle information, yielding 2-D profiles for the neutral density, temperature, and flow velocity. In the second, the kinetic plasma species collide with this neutral fluid background, altering the plasma particle distribution functions in the process.

The effects of the molecules are implicitly incorporated into the built-in kinetic neutral routine by establishing a neutral birth surface in the SOL a finite distance from the vacuum vessel walls (Fig. 1) and launching there atoms with a 3 eV, thermal, isotropic distribution, as if they had been produced by molecular dissociation. For the purposes of this study, we specify a spatial distribution that is peaked around the X-point, as one would expect in a discharge dominated by divertor recycling. Specifically, this distribution is $\propto [1 + 9\exp(-\Delta\theta^2/\Delta\theta_0^2)]$, where the $\Delta\theta$ represents the difference in poloidal angle, measured relative to the magnetic axis-midplane line, between the birth point and the X-point. The width $\Delta\theta_0 = 0.54$ radians is a constant.

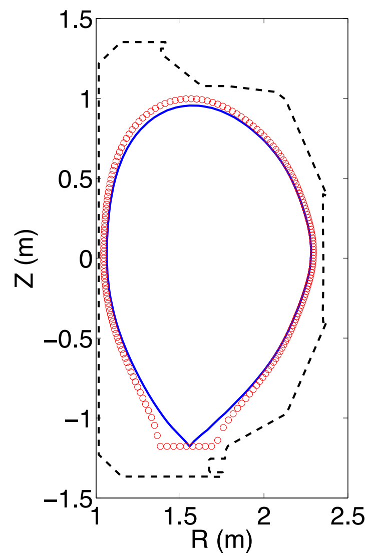

FIG. 1: The dashed lines represent the simulation boundary, determined from the geometry of the DIII-D vacuum vessel. The blue line is the plasma separatrix as specified in the EFIT equilibrium for shot 096333. The red circles delineate the corresponding neutral birth surface.

The atoms are then tracked through the plasma, undergoing ionization and charge exchange along the way. That background plasma is characterized by a Maxwellian distribution, the parameters of which are determined from the current state of the XGC1 (kinetic) plasma. The neutral fluid moments are updated along the tracks.

The ionization rate is specified via the fit:

$$S_{\text{ion}} = 8 \times 10^{-15} \frac{\sqrt{T_e}\exp(-13.56/T_e)}{(1.0 + 0.01T_e)} \text{ m}^3/\text{s}, \quad (1)$$

where T_e is the electron temperature in eV. For $10 < T_e < 10^3$ eV and $n_e < 10^{19}$ m^{-3}, the deviation from a full collisional-radiative result [17] is $< 20\%$; it's uniformly larger for higher densities. The fit used for the CX rate is:

$$S_{\text{cx}} = 1.1 \times 10^{-14} (E_i^{0.3}/\sqrt{M_i}) \text{ m}^3/\text{s}, \quad (2)$$

where E_i is the ion energy or temperature in eV, depending on the application, and M_i is the ion mass in AMU. The deviation from a comprehensive value for the rate, e.g., as in [30], is $< 5\%$ for all atom energies at $T_i = 100$ eV. Generally, the discrepancy is larger for smaller T_i or larger energies, but is only 13% at $T_i = 1$ eV and 3 eV atom energy.

The overall magnitude of the neutral density used in the "kinetic plasma" neutral-plasma collision routine is set so that the volume integrated ionization rate divided by the loss rate of ions to the material surfaces equals the user-specified recycling rate. In our simulation with neutral recycling, this is 99%. The same rate expressions, Eqs. (1) and 2), are used in this routine. The new ions produced by these reactions are sampled from the neutral distribution.

3 Effects on ITG Turbulence

The two simulations documented here are based on a model equilibrium for the DIII-D H-mode shot 96333 [31]. A continuous heating source of 2 MW, consistent with the experimental neutral beam injection rate, is applied in the core region; the associated torque is neglected. No impurity sinks are included.

The initial density and ion temperature profiles, Fig. 2, are specified via analytic expressions calibrated to resemble the profiles used in the EFIT equilibrium calculation. Detailed edge plasma data are not available in this case for both electron and ion temperatures; we make the experimentally relevant assumption that the fixed T_e pedestal is steeper than that of T_i. The full-f XGC1 code quickly evolves the ion temperature and density profiles to a gyrokinetic equilibrium consistent with the specified sources / sinks, ITG and neoclassical transport, and the magnetic field [22]. Given the present focus on ITG turbulence, with the electrons treated adiabatically, the turbulence does not drive any particle transport; the only changes in the ion density profile (and, thus, in the quasi-neutral electron density profile) arise from the sources and sinks. Again, the electron temperature profile is held fixed.

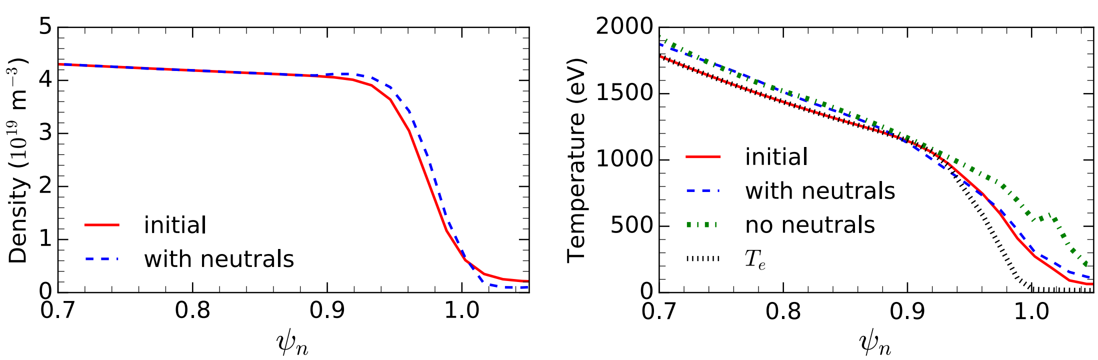

FIG. 2: (a) Initial and final ion density profiles in the with-neutrals run, showing the effects of the neutral ionization source. In the no-neutrals case, the ion density profile remains the same as the initial one. (b) Initial and final ion temperature profiles, along with the (fixed) electron temperature profile.

The 99% recycling simulation ("with-neutrals") is run until the plasma profiles and turbulence self-organize into a quasi-steady state, about 4 ms real time. This state is defined as that in which the relative changes in the plasma and turbulence profiles during a toroidal ion bounce, collision, and turbulence correlation time (all < 0.5 ms) are less than the simulation error [21]. Achieving a perfect steady state is not possible in this short time gyrokinetic simulation since the plasma is evolving on a global transport time scale due to imperfect balances between the sources and sinks, e.g., the less than unity recycling. In the corresponding simulation without recycling ("no-neutrals"), run for 3.4 ms, the ion temperature profile is still evolving at the end, and the SOL density is being depleted due to particle losses to the walls that are not being replenished by neutral ionization.

The flux surface averaged turbulence intensity in the two runs, quantified by $e\sqrt{\langle\phi^2\rangle}/T_e$, with $\langle\phi^2\rangle$ being the RMS average over the flux surface of the deviation of the electrostatic potential from its toroidal mean. As can seen in the comparison depicted in Fig. 3, the saturated turbulence level in the with-neutrals run is the larger of the two. The linear drive for ITG exists at the top of the density pedestal ($\psi_n < 0.92$) where the ion temperature gradient is finite and the density gradient is small, not where the density profile is steep. The turbulence in the latter region is the result of non-local spreading. In the no-neutrals run, the turbulence intensity decreases uniformly with ψ_n.

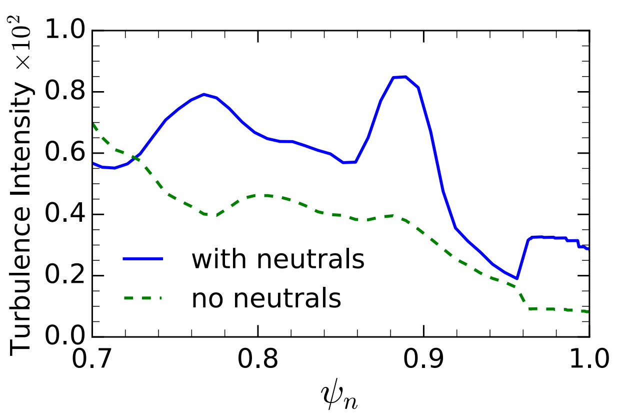

FIG. 3: Turbulence intensity $e\sqrt{\langle\phi^2\rangle}/T_e$ *in the two runs.*

The temporal evolution of the ion temperature profiles (Fig. 2) provides some insight into the origin of this difference in turbulence intensity. The ion temperature gradients for $\psi_n \equiv \psi/\psi_{\rm sep} = 0.85 \rightarrow 1$ in the with-neutrals case are larger than in the no-neutrals run. The profile for the former has saturated to a state that differs only modestly from the initial one while the latter has increased and flattened substantially. Since the only difference between the two simulations is the neutral recycling model, we infer that these effects are associated with the effective ion cooling associated with charge exchange. Note that these effects propagate further into the core than the neutral penetration depth as a result of finite banana orbit mixing, as well as via neoclassical and turbulent transport.

To further quantify this effect, we compute the ITG turbulence drive [32]

$$\eta_i \approx (d\ln T_i/d\psi)/(d\ln n_{e0}/d\psi), \quad (3)$$

where n_{e0} is the initial electron density (Fig. 4). Throughout the runs, the with-neutrals η_i values in the region of interest, $0.85 < \psi_n < 1$, are larger than those in the no-neutrals case.

A second factor contributing to the increase in turbulence intensity with the inclusion of neutral recycling is a reduction in the $E \times B$ shearing rate $dv_{E\times B}/dR$ (Fig. 5) in the steep gradient region, consistent with enhanced non-local edge turbulence in the so-called H-mode layer region [22].

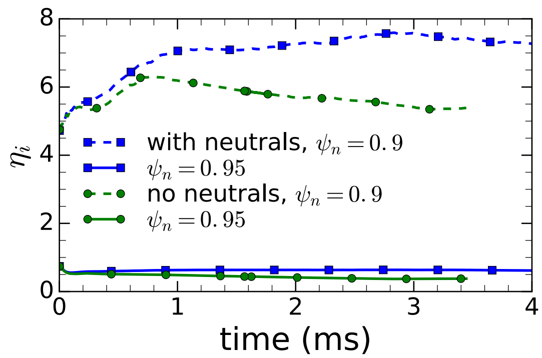

FIG. 4: Temporal evolution of η_i at (a) $\psi_n = 0.9$ and (b) 0.95 in the two simulations.

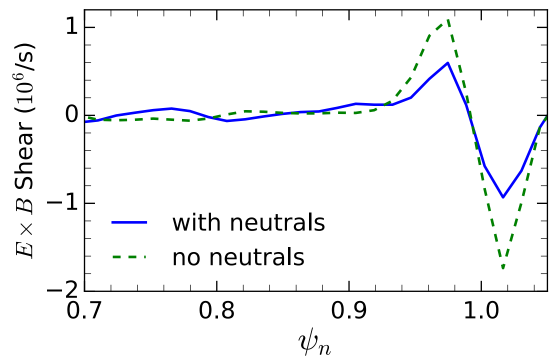

FIG. 5: Radial profiles of $E\times B$ shearing rate in the two simulations.

The connections between sheared $E \times B$, or zonal flows, and L-mode confinement, L-H transition, and internal transport barriers have been the subject of many investigations [33, 34, 35]. For example, a reduction in the zonal flow results in an increase in the L-H power threshold [36]. Analogous damping of the zonal flow rate by the charge exchange friction, and the associated increase in L-H transition power, has been predicted theoretically [5, 6]. The region of reduced $E \times B$ shear overlaps with the neutral penetration zone, suggesting that our result is consistent with those predictions.

4 Conclusions

We have shown that the neutral atoms generated by recycling enhance ITG turbulence through an increase in the ion temperature gradient and a reduction in the $E \times B$ shearing rate. The mean free paths of 3 eV neutral atoms, such as those produced by molecular dissociation, are long enough to reach at least the bottom of the H-mode pedestal. The subsequent ionization and charge exchange reactions alter the ion distribution function there. This, in turn, impacts the ITG turbulence non-locally through neoclassical banana excursion and non-local turbulence interactions. Only with a full-f gyrokinetic simulation, such as that provided by XGC1, can these neoclassical, neutral, and turbulence effects be rendered consistently. Actual comparison of these results with experimental observations to be done in the future will require even more complete simulations. For example, the inclusion of kinetic electrons will allow a consistent evolution of their temperature, as well as both density profiles. The use of a comprehensive neutral transport model, e.g., via DEGAS 2, will provide a consistent neutral source profile and allow molecular processes to be included.

Acknowledgments

This work is supported by U.S. DOE Contract DE-AC02-09CH11466. Most of the support in this contract was provided through the Scientific Discovery through Advanced Computing (SciDAC) program funded by the U.S. DOE Office of Advanced Scientific Computing Research and the Office of Fusion Energy Sciences. Awards of computer time were provided by the Innovative and Novel Computational Impact on Theory and Experiment (INCITE) program. This research used resources of the Argonne Leadership Computing Facility, which is a DOE Office of Science User Facility supported under contract DE-AC02-06CH11357, as well as the National Energy Research Scientific Computing Center, a DOE Office of Science User Facility supported under Contract No. DE-AC02-05CH11231. The lead author wishes to thank R. M. Churchill for his assistance with the XGC1 data files.

References

[1] FÜLÖP, T., et al., Phys. Plasmas 8 (2001) 5214.

[2] FÜLÖP, T., et al., Phys. Rev. Lett. 89 (2002) 225003.

[3] MAINGI, R., et al., Plasma Phys. Control. Fusion 46 (2004) A305.

[4] CAO, B., et al., Plasma Phys. Control. Fusion 54 (2012) 112001.

[5] CARRERAS, B. A., et al., Phys. Plasmas 3 (1996) 4106.

[6] CARRERAS, B. A., et al., Phys. Plasmas 5 (1998) 2623.

[7] GROEBNER, R. J., et al.,Phys. Plasmas 9 (2002) 2134.

[8] D'IPPOLITO, D. A., MYRA, J. R., Phys. Plasmas 9 (2002) 853.

[9] STACEY, W. M., Phys. Plasmas 9 (2002) 3082.

[10] OWEN, L. W., et al., Plasma Phys. Control. Fusion 40 (1998) 717.

[11] COLCHIN, R. J., et al., Nucl. Fusion 40 (2000) 175.

[12] BOIVIN, R. L., et al., Phys. Plasmas 7 (2000) 1919.

[13] FRIIS, Z. W., et al., Phys. Plasmas 17 (2010) 022507.

[14] BATTAGLIA, D. J. et al., Nucl. Fusion 53 (2013) 113032.

[15] VERSLOOT, T. W., et al., Plasma Phys. Control. Fusion 53 (2011) 065017.

[16] ZWEBEN, S. J., et al., Plasma Phys. Control. Fusion 56 (2014) 095010.

[17] STOTLER, D. P., et al., Phys. Plasmas 22 (2015) 082506.

[18] JOHNSON, L. C., HINNOV, E., J. Quant. Spectrosc. Radiat. Transfer 13 (1973) 333.

[19] CHANG, C. S., et al., Phys. Plasmas 11 (2004) 2649.

[20] CHANG, C. S., KU, S., Contrib. Plasma Phys. 46 (2006) 496.

[21] KU, S., et al., Nucl. Fusion 49 (2009) 115021.

[22] CHANG, C. S. et al., Phys. Plasmas 16 (2009) 056108.

[23] LAO, L. L. et al., Nucl. Fusion 25 (1985) 1611.

[24] PARKER, S. E., et al., J. Comp. Phys. 104 (1993) 41.

[25] YOON, E. S., CHANG, C. S., Phys. Plasmas 21 (2014) 032503.

[26] HAGER, R., et al., J. Comp. Phys. 315 (2016) 664.

[27] STOTLER, D. P., KARNEY, C. F. F., Contrib. Plasma Phys. 34 (1994) 392.

[28] STOTLER, D. P., et al., Comput. Sci. Disc. 6 (2013) 015006.

[29] BATTAGLIA, D. J., et al., Phys. Plasmas 21 (2014) 072508.

[30] KRSTIC, P. S., SCHULTZ, D. R., At. Plasma-Mater. Data Fus. 8 (1998) 1, supplement to the journal Nucl. Fus.

[31] OWEN, L. W., et al., J. Nucl. Mater. 290–293 (2001) 464.

[32] HORTON, W., Rev. Mod. Phys. 71 (1999) 735.

[33] DIAMOND, P. H., et al., Plasma Phys. Control. Fusion 47 (2005) R35.

[34] ESTRADA, T., et al., Phys. Rev. Lett. 107 (2011) 245004.

[35] HAHM, T. S., et al., Nucl. Fusion 53 (2013) 093005.

[36] XU, G. S., et al., Phys. Rev. Lett. 107 (2011) 125001.